

Pb-graphene-Pb Josephson junctions: characterization in B field.

I. V. Borzenets, U.C. Coskun, H. Mebrahtu, and G. Finkelstein
Department of Physics, Duke University, Durham, NC 27708

We fabricate superconductor-graphene-superconductor Josephson junctions with superconducting regions made of lead (Pb). The critical current through graphene may be modulated by external magnetic field; the resulting Fraunhofer interference pattern shows several periods of oscillations, indicating that the junction is uniform. Deviations from the perfect Fraunhofer pattern are observed, and their cause is explained by a simulation that takes into account the sample design.

PACS numbers: 74.45.+c, 74.50.+r, 73.23.-b, 72.80.Vp

The properties of superconductor-graphene-superconductor (SGS) junctions have attracted significant attention [1–5]. Unlike the conventional superconductor-normal metal-superconductor (SNS) junctions, devices made with graphene allow for high tunability with the gate voltage. We have recently reported on SGS junctions which use lead (Pb) as the superconducting material [5]. Lead has a relatively high critical temperature of 7.2 K, compared to 1.2 K in the case of the commonly used aluminum. Indeed, we have observed supercurrent through graphene at temperatures as high as 2 K. In this paper, we characterize the properties of these junctions by applying magnetic field.

We fabricate the superconducting contacts to graphene from a Palladium/Lead (Pd/Pb) bilayer. First, we deposit a 2 nm layer of palladium, which creates transparent contacts to graphene [6, 7]; 100nm layer of lead is deposited in situ on top. The lateral width of the contacts is typically 500 nm. In this work we present the results measured on a junction about $20\mu\text{m}$ wide and 400 nm long. (Commonly, length of the junction is defined as the distance between the superconducting contacts, and width as the distance of the normal metal along the superconducting contacts.) In order to create such a wide junction, the leads are bent in two places to fit on a moderately-sized graphene flake (Fig. 1a). We show that this particular sample design has certain nontrivial consequences.

We measured the sample electronic properties using a pseudo 4-probe setup (Fig. 1a). The junction is biased by current I which contains a small AC component, and the AC voltage across the junction is measured using a lock-in amplifier. The carrier density in graphene can be tuned by the back-gate voltage V_{gate} but for the results presented the gate voltage is set at zero. Finally, a perpendicular magnetic field can be applied using two methods. Conventionally, a field B_{ext} can be created by an external solenoid magnet. Alternatively, we send a current I_L along one of the superconducting leads (Fig. 1a), inducing a field which we label as B_L . The advantage of the second method is that the required small fields can be easily obtained and rapidly changed. In this sample we have calibrated B_L to be equal to $0.95\frac{\text{T}}{\text{A}}I_L$ (see

details below).

The Pd/Pb electrodes become superconducting at a temperature of $\approx 7\text{ K}$, and the SGS junctions begin to exhibit enhanced zero-bias conductance at temperatures of $\approx 5\text{ K}$. Below $\approx 2\text{ K}$, a fully formed supercurrent branch is clearly observed [5]. Figure 1c demonstrates the differential conductance $R \equiv dV/dI$ versus bias current I (vertical axis) and magnetic field B_L (horizontal axis) measured at several temperatures. The dark areas of the maps in Figure 1c correspond to the regions of suppressed resistance. The regions are bound by a critical current $I = I_C$, above which the junction becomes normal. The value of I_C increases as temperature is lowered and saturates around $I_C \approx 0.5\mu\text{A}$ at zero magnetic field (see the lowest map in Fig. 1c). When B_L is applied, I_C oscillates in a way closely resembling the Fraunhofer diffraction pattern [10]. Several oscillations of I_C can be observed at the lowest temperature; this indicates that the junction is uniform.

We next apply an external magnetic field B_{ext} , which is found to shift the modulation pattern of Figure 1c in the horizontal direction (Fig. 2). The shift is linear in B_{ext} : indeed, at the center of the pattern the external field and the one induced by I_L cancel each other. The observed rate of shift allows us to fix the conversion $B_L = 0.95\frac{\text{T}}{\text{A}}I_L$ mentioned earlier. This factor is also consistent with our order of magnitude estimates. Furthermore, the shift of the pattern by Φ_0 in an external magnetic field of 0.36 mT allows us to extract the effective area of $5.6\mu\text{m}^2$. While this area is smaller than the $8\mu\text{m}^2$ expected from the designed sample dimensions of $W = 20\mu\text{m}$ by $L = 0.4\mu\text{m}$, it is quite likely that the length L between the leads is reduced in the process of lithography, or that the magnetic field is modified due to the presence of the superconducting leads.

When magnetic field B_{ext} of the order of tens of mT is applied to the sample, the observed pattern becomes distorted even after the field is returned back to zero (Fig. 3). It is clear that the resulting pattern at $B_{ext} = 0$ (Fig. 3a) is very different from the original one (Fig. 2c). We can partially recover the original pattern by setting $B_{ext} \approx 3.4\text{mT}$ (Fig. 3b). When comparing the resulting pattern to the original one (Fig. 2c), we notice that the

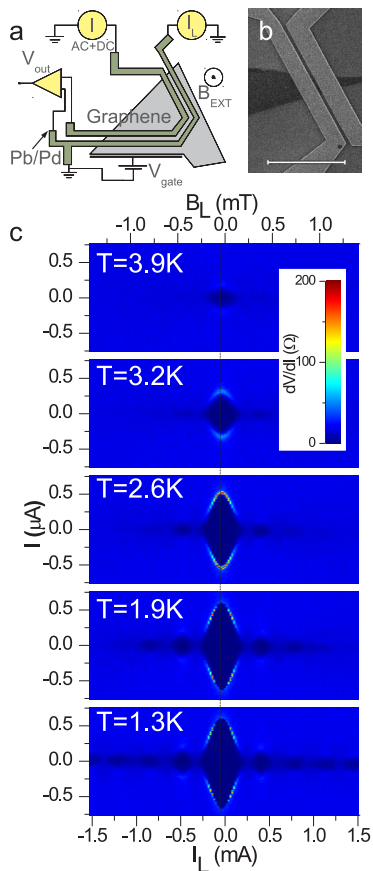


FIG. 1: b) Scanning electron micrograph of a graphene-based SNS Josephson Junction similar but smaller than the one presented in this paper. (Junctions used for measurement were not imaged in order to preserve the quality of graphene.) The dark triangular area is a single layer graphene flake, and the metal contacts are made from lead (Pd) with a thin contact layer of palladium (Pd). a) Schematic of the measurement setup. The metal leads form a "L" shape in order to increase their length. Bias current I is sent through the junction with a small AC component. The resulting AC component of the voltage across the junction is measured using a lock-in amplifier allowing one to record the differential resistance $R \equiv dV/dI$. An external magnetic field B_{ext} is applied by a superconducting solenoid. In addition, a magnetic field B_L is created by sending a current I_L along one of the Pb leads of the junction. Sweeping the current I_L allows to apply a very small magnetic field B_L . c) Differential resistance dV/dI maps measured vs. bias current I and magnetic field-inducing current I_L . Regions of vanishing R appear dark. Each panel corresponds to measurement at a different temperature. Enhanced zero-bias conductance develops around $\approx 4K$ for small fields B_L . With lower temperatures more and more critical current modulations appear and the Fraunhofer interference pattern is observed. At the base temperature of $1.3K$, critical current is seen at fields beyond $5mT$ (only fields up to $1.4mT$ are shown). Observing many oscillations suggest that the junction is highly uniform.

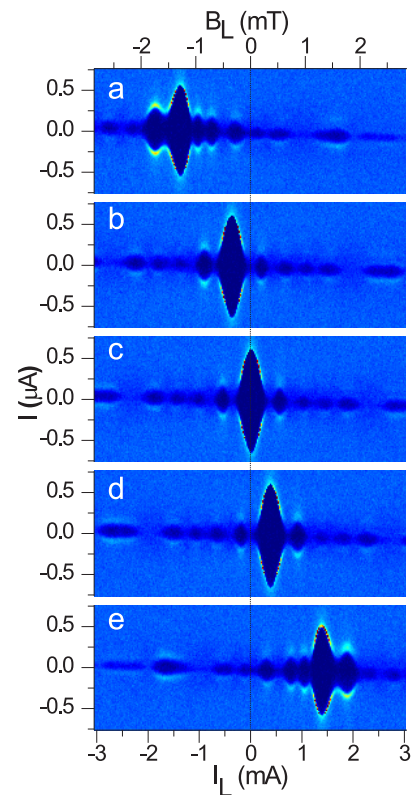


FIG. 2: $R(I, I_L)$ maps (like those in Fig. 1c) measured at different values of the external magnetic field (a): $B_{ext} = -1.3$ mT, (b): $B_{ext} = -0.36$ mT, (c): $B_{ext} = 0$, (d): $B_{ext} = 0.36$ mT, (e): $B_{ext} = 1.3$ mT. Application of B_{ext} shifts the modulation pattern, so that at its center B_{ext} and B_L cancel each other (b-d). Since the cancellation is not perfect, the pattern gets distorted (a), compared to the pattern at zero external field (c). An opposite orientation of the external magnetic field (e) results in mirror reversal of the distortions. $T = 1.3$ K.

critical current is slightly suppressed and the side-lobes have somewhat random heights. We attribute these distortions and the shift from zero field to the trapping of magnetic flux in the superconducting film [11]. Indeed, the undistorted pattern seen in Figure 2c can be restored following the thermal cycling to $\approx 10K$, beyond the critical temperature of lead.

Interestingly, at fields less than those causing trapped flux of Figure 3, distortions of a different nature are introduced to the pattern (Fig. 2a). The first difference is that, returning to $B_{ext} = 0$ restores the original pattern without any hysteresis. Second, the pattern demonstrates perfect symmetry under simultaneous reversal of both B_{ext} and I_L , compare Figures 2 (a) and (e). We associate this behavior with the fact that the phase difference is not linear along the length of the leads. Indeed, the field B_L may not be entirely uniform, so that it is not perfectly compensated by B_{ext} . Most likely, the deviations of B_L from uniformity are caused by the bends in the leads (schematic in Fig. 1a), at which points the

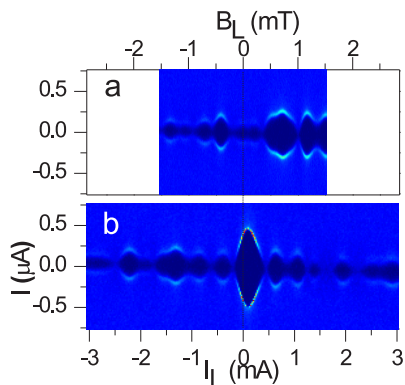


FIG. 3: $R(I, I_L)$ measurements taken after the perpendicular magnetic field was ramped beyond several tens of mT. Panel (a) shows the measurement done when B_{ext} was returned back to zero. Clearly, the pattern is now vastly distorted. Panel (b) is taken at $B_{ext} = 3.4$ mT. At this field, the original critical current modulation pattern (Fig. 2c) is partially restored. However, the central lobe shows a suppressed critical current, and the side-lobes form a distorted pattern. These permanent distortions are attributed to trapped flux in the Pb leads. Heating of the sample beyond the T_C of Pb is required in order to restore the symmetric patterns seen in Figure 2c.

phase difference experiences discontinuous jumps proportional to I_L . The situation is very similar to the junctions with an artificial phase discontinuity controlled by an external current [12, 13]. Indeed, some of the features we observe in Figures 2(a) and (e), *e.g.* the strengthening of the side lobe at the expense of the central lobe, resemble those found in Refs. [12, 13].

To describe the distortions found in Figure 2a,e, we consider a semi-realistic model of the sample. We assume that the leads extend from $x = -W/2$ to $+W/2$; the position-dependent phase difference $\Phi_L(x)$ (induced by $B_L(x)$) is taken to be piece-wise linear in x , with a slope proportional to I_L . Two identical discontinuous jumps of $\Phi_L(x)$ are placed at $-W/10$ and $+W/10$. The strength of the discontinuities is taken to be also proportional to I_L . These points are close to the actual locations of the bends in the leads, but we checked that the main features of the simulation do not crucially depend on the details (*i.e.* the position of discontinuities or symmetry of their placement).

We also include the effect of the external field, presuming it induces uniform phase difference $\Phi_{ext}(x)$ along the length of the leads. In our simulations, the current-phase relation is assumed to be sinusoidal. Although deviations from a sinusoidal relation have been recently observed in SGS junctions [14], the approximation should be adequate in our case, due to the relatively large length between the leads ($L = 400$ nm) and the relatively high temperature $\gtrsim 1$ K.

The simulated patterns of the critical current I_C vs. I_L and B_{ext} are shown in Figure 4. The main features

observed in Figure 2 are qualitatively reproduced, such as: 1) the overall shift of the $I_C(I_L)$ pattern in B_{ext} ; 2) the growing distortion of the $I_C(I_L)$ pattern in B_{ext} ; 3) the growing strength of the side lobe on the high current side of the pattern at the expense of the central lobe; 4) the difference in width between that side lobe and the side lobes on the other side. Moreover, even the $B_{ext} = 0$ curve, while similar to the perfect Fraunhofer pattern $I \propto \sin(\pi I_L/I_L^{(0)})/I_L$, bears noticeable differences. Namely, some of the side lobes are suppressed almost to zero, while further lobes at higher I_L regain strength. This type of behavior is indeed observed in experiment (Fig. 5). Note the region of suppressed critical current at $I_L \approx \pm 2.3$ mA in Figure 2c, and its reappearance at higher $I_L \approx \pm 3.5$ mA.

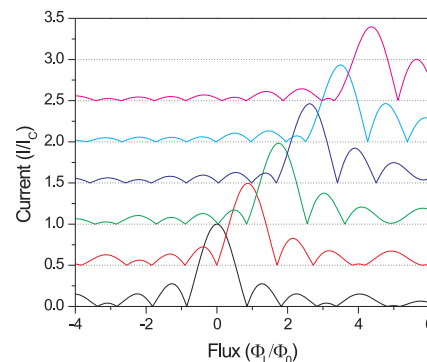


FIG. 4: Simulated critical current vs. I_L at several values of B_{ext} . The bottom curve is taken at $B_{ext} = 0$, and in each consecutive curve the external flux grows in units of flux quantum Φ_0 . The phase difference between the two leads induced by I_L is assumed to grow linearly along the length of the leads, proportionally to I_L , and to jump discontinuously at two locations by an amount also proportional to I_L . This particular functional form is chosen to approximate the realistic shape of the sample, where the leads turn 90° in two places; however the major features appear insensitive to the exact locations of the discontinuities. The horizontal axis is labeled in units of total flux Φ_L induced by I_L excluding the discontinuities. The additional phase jump at each discontinuity is equal to $0.1\pi\Phi_L/\Phi_0$.

In conclusion, we demonstrate magnetic field-induced quasi-periodic modulation of critical current in Pb-graphene-Pb structures, which indicates their spatial uniformity. The magnetic field can be applied by running a current through one of the superconducting leads within the same structure, resulting in a simple, yet efficient method to *in situ* control the critical current. The dependence of the critical current on thus applied magnetic field deviates from the perfect Fraunhofer interference pattern. The difference is attributed to the presence of bends in the superconducting leads; a simple simulation supports this explanation.

The work was supported by the U.S. Department of

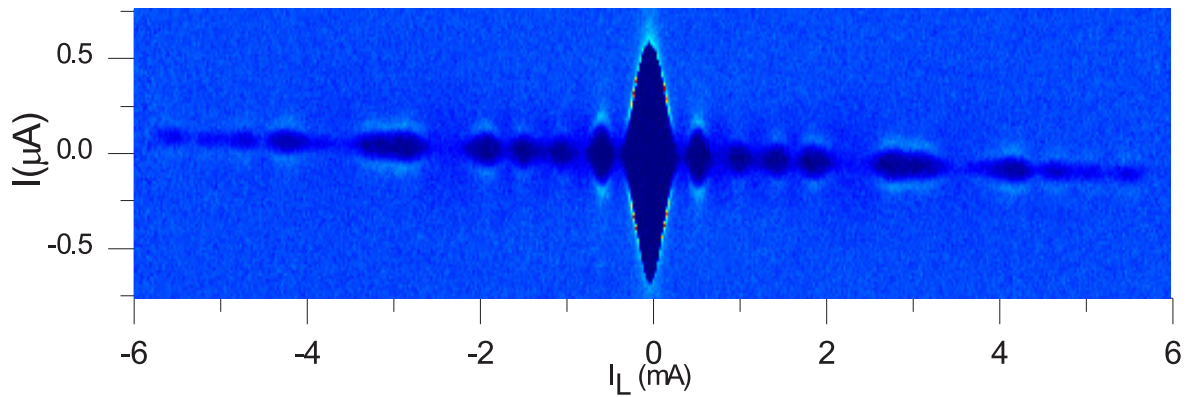


FIG. 5: Differential resistance dV/dI map measured vs. bias current I and current I_L inducing magnetic field. This data are similar to Fig. 2c, but is extended up to $I_L = 6mA$. Note the suppression of select side-lobes (see $I_L \approx \pm 2.5mA$ and $\pm 3.5mA$). This suppression of side-lobes qualitatively resembles the simulation results (Fig. 4, $B_{ext} = 0$, $\Phi_L/\Phi_0 \approx \pm 3$ and ± 5). The tilt of the pattern is an artifact of I_L flowing through the normal part of the sample, thus creating a voltage drop that shifts the zero of I .

Energy, Office of Basic Energy Sciences, Division of Materials Sciences and Engineering under Award de-sc0002765.

-
- [1] H. B. Heersche, P. Jarillo-Herrero, J. B. Oostinga, L. M. K. Vandersypen, and A. F. Morpurgo, *Nature* **446**, 56 (2007).
 - [2] F. Miao, S. Wijeratne, Y. Zhang, U. C. Coskun, W. Bao, and C. N. Lau, *Science* **317**, 1530 (2007).
 - [3] X. Du, I. Skachko, and E. Y. Andrei, *Phys. Rev. B* **77**, 184507 (2008).
 - [4] C. Ojeda-Aristizabal, M. Ferrier, S. Gueron, and H. Bouchiat, *Phys. Rev. B* **79**, 165436 (2009).
 - [5] I. V. Borzenets, U. C. Coskun, S. J. Jones, and G. Finkelstein, *Phys. Rev. Lett.* **107**, 137005 (2011)
 - [6] B. Huard, N. Stander, J. A. Sulpizio, and D. Goldhaber-Gordon, *Phys. Rev. B* **78**, 121402 (2008).

- [7] F. Xia, V. Perebeinos, Y. Lin, Y. Wu, and P. Avouris, *Nature Nano.* **6**, 179 (2011).
- [8] K. S. Novoselov, D. Jiang, F. Schedin, T.J. Booth, V. V. Khotkevich, S. V. Morozov, and A. K. Geim, *PNAS* **102**, 10451 (2005).
- [9] A. C. Ferrari, J. C. Meyer, V. Scardaci, C. Casiraghi, M. Lazzeri, F. Mauri, S. Piscanec, D. Jiang, K. S. Novoselov, S. Roth, and A. K. Geim, *Phys. Rev. Lett.* **97** 187401, (2006).
- [10] M. Tinkham, *Introduction To Superconductivity* (McGraw-Hill, 1996).
- [11] S. L. Miller, K. R. Biagi, J. R. Clem, and D. K. Finnemore, *Phys. Rev. B* **31**, 268 (1985).
- [12] T. Gaber, E. Goldobin, A. Sterck, R. Kleiner, D. Koelle, M. Siegel, and M. Neuhaus, *Phys. Rev. B* **72**, 054522 (2005).
- [13] E. Goldobin, A. Sterck, T. Gaber, D. Koelle, and R. Kleiner, *Phys. Rev. Lett.* **92**, 057005 (2004).
- [14] C. Chialvo, I. C. Moraru, D. J. Van Harlingen, and N. Mason, arXiv:1005.2630v2 (2010)